EUROPEAN JOURNAL OF PURE AND APPLIED MATHEMATICS
2025, Vol. 18, Issue 3, Article Number 6260
ISSN 1307-5543 – ejpam.com
Published by New York Business Global

Numerical Investigation of MHD Flow of a Tangent Hyperbolic Fluid in a Porous Medium with Viscous Dissipation, Soret and Dufour Effects

K Umamaheswara Rao[1], Siva Reddy Sheri[2], Srinivas Reddy Kallem[2,*], Alfunsa Prathiba[3], Shankar Gollapalli[4], Medhat M. Helal[5,7], A. I. Ismail[6,7]

[1] *Department of Mathematics, HITAM, Hyderabad, Telangana, India*
[2] *Department of Mathematics, GITAM (Deemed to be University), Hyderabad, Telangana, India*
[3] *Department of Mathematics, CVR College of Engineering, Hyderabad, Telangana, India*
[4] *Department of Mathematics, B V Raju Institute of Technology, Narsapur, Medak, Telangana-502313,India*
[5] *Civil Engineering Department, College of Engineering and Architecture, Umm Al-Qura University, Makkah, Saudi Arabia*
[6] *Department of Mathematics, Faculty of science Tanta University, 31527, Egypt*
[7] *Department of Engineering Mathematics and Physics, Zagazig University, Zagazig, Egypt*

Abstract. A numerical analysis was performed on the steady-state magnetohydrodynamics of a tangent hyperbolic nanofluid (THNF) flowing over a vertically expanding surface with nonlinear expansion. This study examines the influence of factors such as sheet thickness variation, Darcy number, magnetic field, heat source/sink, thermal conductivity, viscous dissipation, and thermal radiation on THNF flow behavior. The THNF model, classified as a non-Newtonian fluid, is widely utilized in laboratory settings and industrial machinery for the management of excessive heat. The governing equations were non-dimensionalized and transformed into a system of ordinary differential equations (ODEs) using similarity variables to evaluate the flow. The ordinary differential equations were solved numerically using the MATLAB BVP4C solver. A comparative evaluation was conducted to assess the accuracy of the results. Graphical analysis demonstrated that activation energy increases the rate of mass transfer, while chemical reactions typically reduce it. The research also demonstrated that the Weissenberg number, Brownian motion, and Rayleigh number collectively increase the fluid temperature. Furthermore, increasing the Darcy number and thermal radiation improved fluid flow and heat transfer rates, respectively. Skin friction increased with higher Ec and magnetic field intensity, even though the rate of energy transmission decreased.

2020 Mathematics Subject Classifications: 76-11, 76A05, 76B75, 76D10, 76D10, 76W05
Key Words and Phrases: Hyperbolic tangent fluid, Viscous dissipation, Soret number, Dufour number, Magnetic field

*Corresponding author.
DOI: https://doi.org/10.29020/nybg.ejpam.v18i3.6260

Email addresses: umasirmaths@gmail.com (Umamaheswara), skallem@gitam.in (S. R. Kallem), ssheri@gitam.edu (S. R. Sheri), alfunsaperli@gmial.com (A. Prathiba), gollapallishankar935@gmail.com (G.Shankar), mmhelal@uqu.edu.sa (M. M. Helal), aiismail@uqu.edu.sa (A. I. Ismail)

1. Introduction

Tangent hyperbolic non-Newtonian fluids (THNFs) include various fluid types, each characterized by distinct properties. Among non-Newtonian fluids, THNFs are notable for their precise mathematical model, which provides benefits including tangible determination, intuitive behavior, and efficient computation. Common substances such as ashes, vinegar, bloodstream fluid colorants, and whipped cream fall under this category. Recent studies by researchers globally have extensively examined THNFs, investigating their behavior under different scenarios and influencing factors. The incorporation of tiny particles in a cooling water nuclear system markedly improves safety margins and offers substantial economic advantages [1–6].

Research has investigated the magnetohydrodynamics (MHD) of THNFs over stretching sheets. Mahdy and Chamkha [7] employed the Keller box procedure to mathematically model the boundary layer flow (BLF) of dual-phase THNFs across an extended wedge in a porous medium. Atif et al. [8] adopted the shooting method to examine the mass and heat transfer in THNFs surrounding a sheet. Both studies, however, did not consider critical parameters such as wall porosity, buoyancy-induced forces, viscous dissipation, Joule heating, and internal heat generation.

Nadeem and Akbar [9] developed an alteration method to simulate the movement of THF within a uniform tube. Building upon earlier research [10], Nadeem and Akram [10] examined the impact of partial slip in an asymmetrical channel and formulated perturbation methods for the governing equations. Gireesha and Goutham [11] explored stretched flows of THFs using the collocation method. Akbar et al. [12] conducted a numerical investigation of boundary layer flow over a stretching sheet in the presence of a magnetic field, revealing that the Hartmann number and Weissenberg number hinder fluid motion. Malik et al. [13] studied THF flow over a stretched cylinder and derived solutions using the Keller box method. Waqas et al. [14] applied the generalized Fourier heat law to analyze THF flow over a nonlinear stretching sheet, employing the Homotopy Analysis Method (HAM) to find an array solution for a boundary value problem. Rehman et al. [15] examined the influence of heat radiation [16, 17] on THF flow over smooth and cylindrical surfaces.

Salahuddin et al. [18] and Varsha et al. [19] explored the MHD movement of THFs along an elongating cylinder, accounting for exponentially varying thermal conductivity and opposing magnetic fields. Azam et al. [20] statistically studied cross-nanofluid motion around a moving cylinder, considering varying thermal characteristics and the presence of an energy source or sink. Bibi et al. [21] examined instability migration and radiated boundary effects in THFs with variable thermal conductivity. Shutaywi et al. [22] investigated ferrofluid flow across a porous paraboloid surface, incorporating variable fluid properties, entropy production, and temperature effects.

Patra et al. [23] examined the unstable Falkner–Skan motion of THNF along a stretching sheet, considering chemical reactions and activation energy. Their results suggest that increased reaction rates reduce nanoparticle concentration, while higher activation energy increases it. Ullah et al. [24] studied the effects of suction and injection on 2D MHD hyper-

bolic fluid flow along a boundary, concluding that increased suction/injection parameters decrease both acceleration and boundary layer thickness.

Oyelakin and Sibanda [25] analyzed the influence of exponentially varying thermal conductivity, magnetic field strength, and viscosity on hyperbolic fluids. They demonstrated that reducing viscosity lowers flow resistance and enhances velocity, while temperature and species concentration profiles decrease. Kumar et al. [26] investigated the effects of activation energy on THF flow over a moving stretching sheet, finding that the velocity increases with the higher Weissenberg number and the heat transfer rates improve with higher values of radiation parameters. Noor et al. [27] studied MHD flow in a viscous fluid through a non-Darcian porous medium adjacent to stretched sheets with permeable and impermeable surfaces.

Ramly et al. [28] explored axisymmetric fluid flow saturated with nanoparticles under thermal radiation, integrating both active and passive nanoparticle control. Their findings suggest that thermophoresis significantly improves heat conduction, especially under passive nanoparticle control.

This study focuses on the steady magnetohydrodynamic (MHD) flow and heat transfer characteristics of a tangent hyperbolic nanofluid over a stretching sheet embedded in a porous medium. The investigation incorporates complex physical effects, including viscous dissipation, Soret and Dufour effects, internal heat generation or absorption, and magnetic field influence. Despite extensive prior work by Amer et al. [29] and Kallem et al. [30] on non-Newtonian fluids, limited attention has been paid to the combined effects of these parameters, especially in the context of tangent hyperbolic fluids in porous media under MHD and radiative environments.

To address this gap, the governing partial differential equations are transformed into a system of coupled nonlinear ordinary differential equations and solved numerically using MATLAB's `bvp4c` solver. The study systematically analyzes the effects of key physical parameters on the velocity, temperature, and nanoparticle concentration profiles. The results are presented graphically to enhance understanding of heat and mass transfer mechanisms in such complex flow systems.

2. Problem Statement

This research examines the two-dimensional, steady, incompressible flow of a tangent hyperbolic nanofluid over a porous stretching sheet, as well as the effects of an angled magnetic field. The deformable surface is positioned at $y = 0$, and the magnetic force is applied at an inclined angle γ. The velocity components are denoted by u and v in the physical model illustrated in Fig. 1.

Furthermore, the study explores the influences of viscosity, Soret number, and Dufour number on the flow and thermal characteristics. Table 1 presents the precision and consistency of the computational method employed, by comparing the values of $f''(0)$ for the case where $\mathrm{We} = n = \mathrm{Da} = 0$ and $\gamma = \pi/2$, with the reference data available in the literature for the limit scenario. This comparison serves to validate the numerical approach used to solve the governing equations.

The system of equations is formulated based on the assumptions outlined in our study, consistent with the methodology demonstrated in the earlier works of Pasha et al. [31].

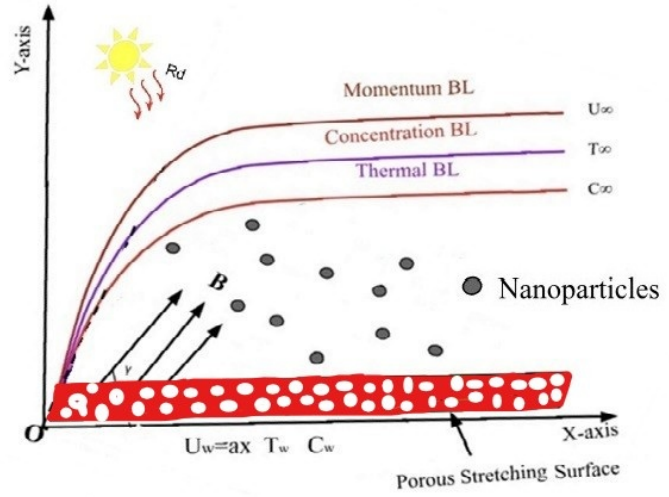

Figure 1: Fluid flow near porous stretching sheet.

The governing equations for the steady, incompressible tangent hyperbolic nanofluid flow with inclined magnetic field and porous media are:

$$\frac{\partial u}{\partial x}+\frac{\partial v}{\partial y}=0 \tag{1}$$

$$u\frac{\partial u}{\partial x}+v\frac{\partial u}{\partial y}=\vartheta\left[(1-n)+\sqrt{2}n\Gamma\frac{\partial u}{\partial y}\right]\frac{\partial^2 u}{\partial y^2}-\frac{\sigma}{\rho}uB_0^2(x)\sin^2\gamma-\frac{\vartheta}{K}u \tag{2}$$

$$\begin{aligned}u\frac{\partial T}{\partial x}+v\frac{\partial T}{\partial y}=&\alpha\frac{\partial^2 T}{\partial y^2}+\frac{\mu}{\rho c_p}\left(\frac{\partial u}{\partial y}\right)^2+\frac{D_m K_T}{c_s c_p}\frac{\partial^2 C}{\partial y^2}\\&+\frac{16\sigma^* T_\infty^3}{3k^*\rho c_p}\frac{\partial^2 T}{\partial y^2}+\frac{Q_0}{\rho c_p}(T-T_\infty)\end{aligned} \tag{3}$$

$$u\frac{\partial C}{\partial x}+v\frac{\partial C}{\partial y}=\frac{D_T K_T}{T_\infty}\frac{\partial^2 T}{\partial y^2}+D_B\frac{\partial^2 C}{\partial y^2}-K_r(C-C_\infty) \tag{4}$$

Boundary Conditions [32]

$$\begin{cases}u=u_w(x)=ax, \quad v=0, \quad T=T_w, \quad C=C_w & \text{at } y=0\\ u\to 0, \quad T\to T_\infty, \quad C\to C_\infty & \text{as } y\to\infty\end{cases} \tag{5}$$

Similarity Transformations

Using the following similarity transformations:

$$\begin{aligned} u &= \frac{\partial \Psi}{\partial y} = axf'(\eta), \\ v &= -\frac{\partial \Psi}{\partial x} = -\sqrt{a\vartheta} f(\eta), \\ \Psi &= \sqrt{a\vartheta} x f(\eta), \\ \eta &= \sqrt{\frac{a}{\vartheta}} y, \quad g(\eta) = \frac{C - C_\infty}{C_w - C_\infty}, \quad \theta(\eta) = \frac{T - T_\infty}{T_w - T_\infty} \end{aligned} \tag{6}$$

Reduced Dimensionless Equations

Substituting into the governing equations yields the following.

$$\left[(1-n) + nWef''\right] f''' + f''f - (f')^2 - Daf' - M\sin^2\gamma\, f' = 0 \tag{7}$$

$$\left(1 + \frac{4R}{3}\right)\theta'' + Pr\left(D_f g'' - \theta' f + Q\theta + Ec(f'')^2\right) = 0 \tag{8}$$

$$g'' + Sc\left(Sr\theta'' + g' - \gamma_1 g\right) = 0 \tag{9}$$

The dimensionless boundary conditions are:

$$\begin{cases} f' = 1, \quad f = 0, \quad \theta = 1, \quad g = 1 & \text{at } \eta = 0 \\ f' \to 0, \quad \theta \to 0, \quad g \to 0 & \text{as } \eta \to \infty \end{cases} \tag{10}$$

The non-dimensional parameters are defined as follows:

$$\begin{aligned} We &= \sqrt{\frac{2a^3}{\vartheta}}\,\Gamma && \text{(Weissenberg number)} \\ n &= \text{power-law index} \\ Da &= \frac{\vartheta}{aK} && \text{(Darcy number)} \\ M &= \frac{\sigma B_0^2(x)}{a\rho} && \text{(Magnetic parameter)} \\ \gamma &= \text{Inclined angle of magnetic field} \\ R &= \frac{4\sigma^* T_\infty^3}{kk^*} && \text{(Radiation parameter)} \\ Pr &= \frac{\vartheta}{\alpha} && \text{(Prandtl number)} \end{aligned}$$

$$D_f = \frac{D_m K_T (C_w - C_\infty)}{c_s c_p (T_w - T_\infty)\vartheta} \quad \text{(Dufour number)}$$

$$Q = \frac{Q_0}{a\rho c_p} \quad \text{(Heat source parameter)}$$

$$Ec = \frac{u_w^2}{c_p (T_w - T_\infty)} \quad \text{(Eckert number)}$$

$$Sc = \frac{\vartheta}{D_B} \quad \text{(Schmidt number)}$$

$$Sr = \frac{D_T K_T (T_w - T_\infty)}{\vartheta T_\infty (C_w - C_\infty)} \quad \text{(Soret number)}$$

$$\gamma_1 = \frac{k^*}{a} \quad \text{(Reaction variable)}$$

The mathematical expressions for the dimensionless quantities are[33]:

$$C_f = \frac{\tau_w}{\rho u_w^2}, \quad \tau_w = \mu \left.\frac{\partial u}{\partial y}\right|_{y=0}, \quad C_f \sqrt{Re_x} = \left[(1-n) + \frac{n}{2} We f''(0)\right] f''(0) \tag{11}$$

$$Nu_x = \frac{x q_w}{k(T_w - T_\infty)}, \quad q_w = -k \left.\frac{\partial T}{\partial y}\right|_{y=0}, \quad \frac{Nu_x}{\sqrt{Re_x}} = -\theta'(0) \tag{12}$$

$$Sh_x = \frac{x q_s}{D_B (C_w - C_\infty)}, \quad q_s = -D_B \left.\frac{\partial C}{\partial y}\right|_{y=0}, \quad \frac{Sh_x}{\sqrt{Re_x}} = -g'(0) \tag{13}$$

where the local Reynolds number is given by:

$$Re_x = \frac{u_w x}{\vartheta} \tag{14}$$

2.1. Numerical Method

The severely complex unitless modified system of equations (7)–(9), together with the boundary conditions in (10), constitute a two-point boundary value problem (BVP). Complex governing equations are often more difficult to solve analytically than numerically. Among the several numerical methodologies available, the `bvp4c` method distinguishes itself due to its simplicity of implementation and its ability to handle challenging boundary conditions.

To obtain the numerical solution, we used the `bvp4c` solver available in MATLAB, and the corresponding computational process is illustrated in Fig. 2. Since `bvp4c` is designed to solve first-order ordinary differential equations (ODEs), the dimensionless governing equations and their associated boundary conditions must be reformulated—using similarity transformations [30, 34–36]—into a system of first-order ODEs.

The solver `bvp4c` iteratively refines the mesh and converges when the difference between the computed solution and the exact equations is within a specified tolerance, typically 10^{-4}. It automatically adds points where necessary to ensure high accuracy.

We define the following substitutions:

$$\begin{aligned}
x_1 &= f(\eta), & x_1' &= x_2,\\
x_2 &= f'(\eta), & x_2' &= x_3,\\
x_3 &= f''(\eta), & x_3' &= \frac{x_2^2 + M\sin^2\gamma\, x_2 - x_1 x_3 + Da\, x_2}{(1-n) + n\, We\, x_3},\\
x_4 &= \theta(\eta), & x_4' &= x_5,\\
x_5 &= \theta'(\eta), & x_5' &= \frac{Pr\left(x_1 x_5 - D_f\, x_7' - Q\, x_4 - Ec\, x_3^2\right)}{1 + \frac{4R}{3}},\\
x_6 &= g(\eta), & x_6' &= x_7,\\
x_7 &= g'(\eta), & x_7' &= Sc\left(\gamma_1 x_6 - x_7 - Sr\, x_5'\right).
\end{aligned}$$

The boundary conditions for the above system are the following:

$$\begin{aligned}
x_1(0) &= 0, & x_2(0) &= 1, & x_3(0) &= b_1,\\
x_4(0) &= 1, & x_5(0) &= b_2, & &\\
x_6(0) &= 1, & x_7(0) &= b_3, & &\\
x_2(\infty) &\to 0, & x_4(\infty) &\to 0, & x_6(\infty) &\to 0.
\end{aligned}$$

This study has valuable applications in areas such as electronic cooling (e.g., CPUs, power devices), thermal management in porous heat exchangers, and biomedical fields including drug delivery and hyperthermia therapy. Additionally, it supports enhanced process control in material processing and metallurgy, and contributes to improved energy efficiency in environmental and solar energy systems through a better understanding of heat and mass transfer in complex flows.

The `bvp4c` method used in this study offers strong capabilities for solving nonlinear, coupled, and steady-state boundary value problems with adaptive precision. Its efficiency, reliability, and flexibility make it highly suitable for modeling complex physical phenomena such as MHD flow, and heat and mass transfer in porous media and nanoparticle-enhanced fluids.

3. Findings and Analysis

This portion delineates the quantitative and qualitative findings obtained from the analysis of the inclined magnetohydrodynamic (MHD) flow of a hyperbolic tangent fluid (HTF) over a stretching sheet (SS) embedded in a porous medium. The effects of key factors such as the power-law exponent, Soret and Dufour numbers, Weissenberg number (We), magnetic field strength (M), inclination angle (γ), radiation parameter (R), heat source parameter (Q), Eckert number (Ec), Prandtl number (Pr), Schmidt number (Sc), and reaction rate constant (Rc) are systematically analyzed on the concentration, velocity,

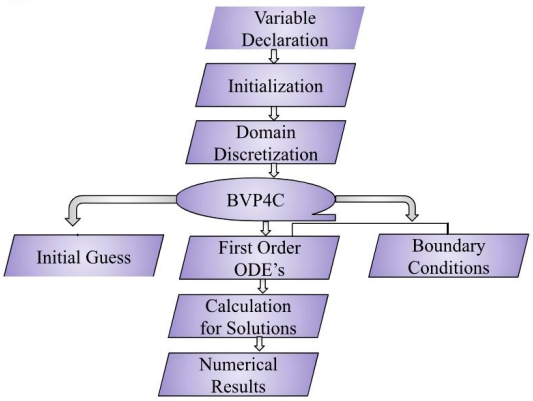

Figure 2: Flow chart of the numerical solution procedure.

Table 1: Comparative Table for the Newtonian Case When $We = n = Da = 0$ and $\gamma = \frac{\pi}{2}$.

M	Waqas.et.al., [37]	Amer et.al., [29]	Khalid et.al [38]	Present Study
0	-1	-1	-1.0001	-1.001
0.5	-1.1180	-1.1180	-1.2247	-1.2250
1	-1.4142	-1.4139	-1.4142	-1.4145
5	-2.4495	-2.4495	-2.4495	-2.4495
10	-3.3166	-3.3166	-3.3166	-3.3166
100	-10.0499	-10.0499	-10.0499	-10.0499
500	-22.3830	-22.3830	-22.3830	-22.3830
1000	-31.6386	-31.6386	-31.6386	-31.6386

and temperature fields. All computations are carried out using MATLAB's boundary value problem solver `bvp4c`. The inclination angle (γ) of the magnetic field has a pronounced effect on the velocity, temperature, and concentration distributions in hyperbolic tangent fluid flow. As shown in Fig. 3, increasing γ reduces the fluid velocity due to the added resistive influence of gravitational and inertial forces along the inclined magnetic field. Figure 4 further reveals that the temperature profile decreases with higher γ, indicating enhanced thermal resistance and a thinner thermal boundary layer. Moreover, Fig. 5 shows that concentration also diminishes with increasing inclination angle, highlighting the coupling between thermal and solutal transport.These findings emphasize the significance of magnetic field strength and inclination angle in industrial applications such as materials processing and advanced cooling technologies. The power-law exponent (n) significantly affects the velocity and thermal profiles of the fluid. Fig. 6 and Fig. 7 reveal that increasing n reduces the fluid velocity near the stretching sheet, indicating a greater resistance to flow. Simultaneously, the temperature profile also decreases with increased n, suggesting a thinner thermal boundary layer. This behavior is consistent with the non-Newtonian characteristics of hyperbolic tangent fluids, where larger n values correspond to increased viscosity. The resulting higher viscous forces impede both flow and heat transfer. However,

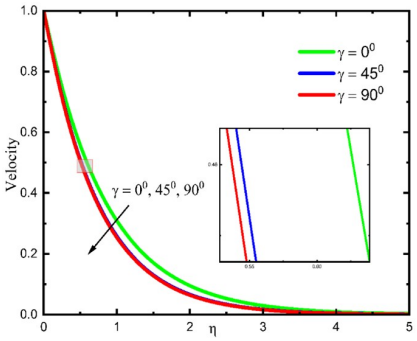

Figure 3: Variation of γ on Velocity.

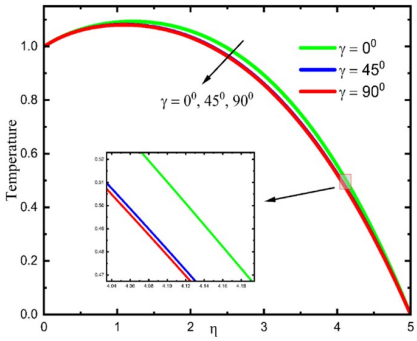

Figure 4: Variation of γ on Temperature.

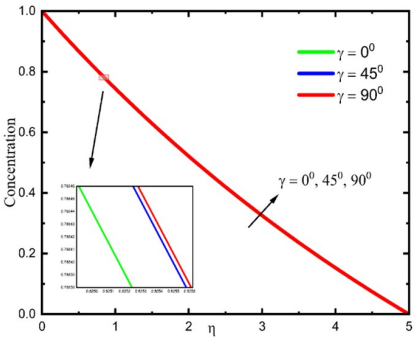

Figure 5: Effect of γ on Concentration profile

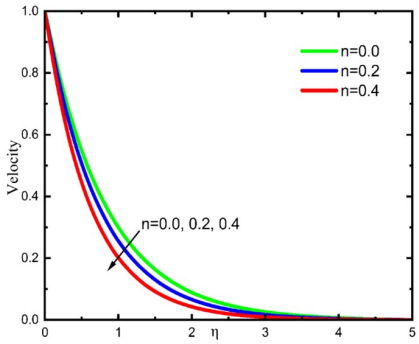

Figure 6: Effect of n on Velocity profile

this trend contrasts with the behavior of the concentration profile, as indicated in Fig. 8, where an increase in n leads to an increased species concentration near the surface.

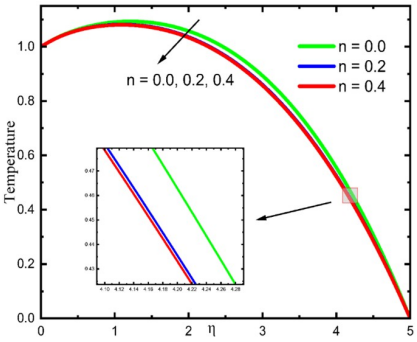

Figure 7: Variation of n on Temperature

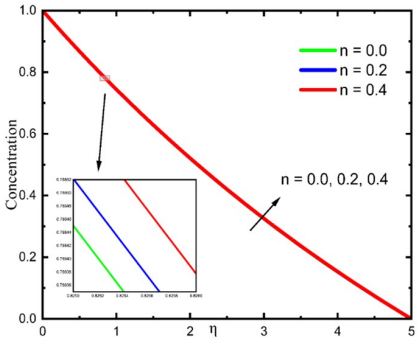

Figure 8: Variation of n on Concentration

The Weissenberg number (We), which represents the elastic effects of the fluid, has a noticeable impact on velocity profiles. Figures 9 and 10 demonstrate that increasing We reduces both the temperature and velocity, particularly near the stretching sheet, as elastic forces begin to dominate the fluid dynamics. This effect is more pronounced for fluids exhibiting strong non-Newtonian behavior, highlighting the critical role of We in engineering applications involving hyperbolic tangent fluids. Furthermore, the Weissenberg number (We), associated with fluid elasticity, significantly alters the concentration profile,

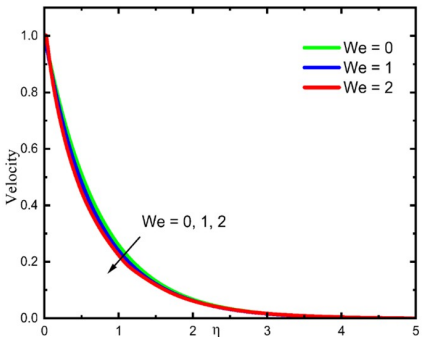

Figure 9: Variation of We on Velocity

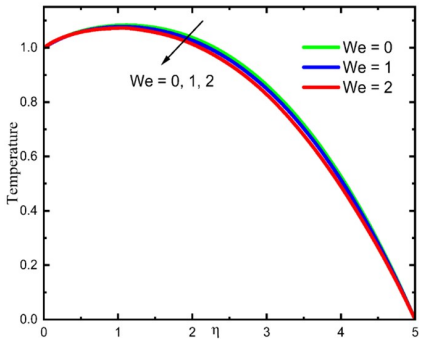

Figure 10: Variation of We on Temperature

as illustrated in Figure 11. An increase in We leads to higher concentration levels near the sheet, as elastic forces interfere with mass transfer within the boundary layer. This results in a thicker solutal boundary layer, especially in fluids with pronounced non-Newtonian characteristics. Higher Darcy number (Da) values reduce the porous flow capacity, thereby

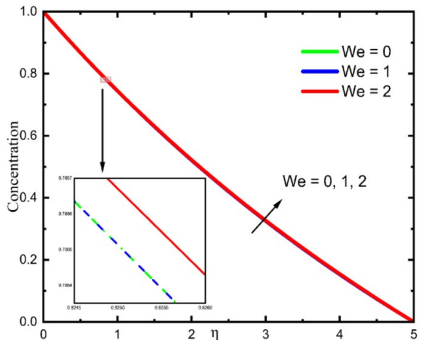

Figure 11: Variation of We on Concentration

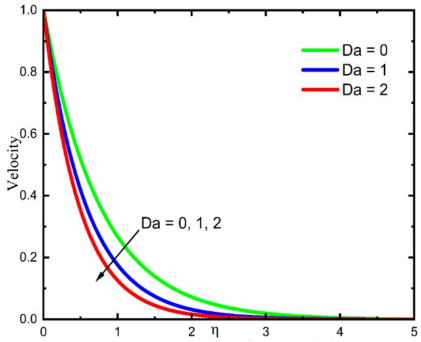

Figure 12: Variation of Da on Velocity

increasing obstruction to fluid momentum, as seen in Figure 12, where velocity decreases, particularly near the sheet. Similarly, Figure 13 shows that higher Da facilitates heat dissipation via enhanced convection, leading to lower temperature profiles and a thinner thermal boundary layer. Regarding concentration, Figure 14 indicates that increased Da enhances mass transfer, raising concentration levels near the sheet and thickening the solutal boundary layer. The magnetic field strength (M) plays a crucial role in controlling the flow characteristics. As shown in Figures 15 and 16, higher M values reduce both velocity and temperature due to the magnetoelectric (Lorentz) force, which acts as a resistive drag on fluid motion. These findings underscore the significance of magnetic field strength and orientation in applications such as materials processing and cooling technologies. Furthermore, the parameter M influences concentration profiles indirectly by modifying the flow dynamics. As illustrated in Figure 17, higher M values enhance concentration levels by restricting fluid motion through the Lorentz force, which amplifies convective transport mechanisms. The effect of radiation (R) on the behavior of hyperbolic tangent fluids reveals a different trend than initially expected. As shown in Figure 18, the velocity profile decreases with increasing R, which can be attributed to the lowered fluid temperature.

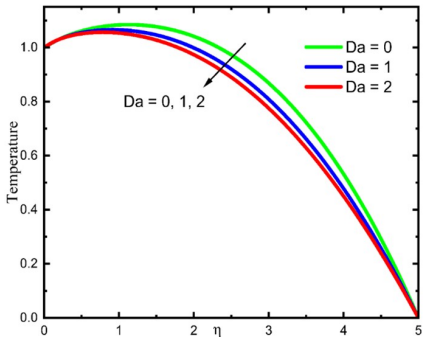

Figure 13: Variation of Da on Temperature

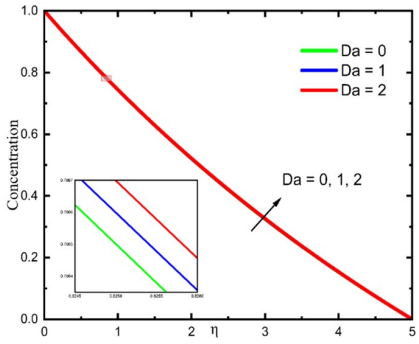

Figure 14: Variation of Da on Concentarion

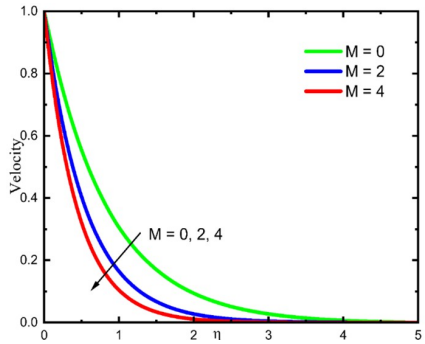

Figure 15: Variation of M on Velocity

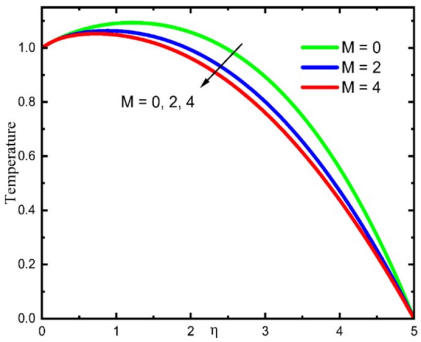

Figure 16: Variation of M on Temperature

This reduction in temperature increases the viscosity and dampens the flow motion. Additionally, the thinner thermal boundary layer reduces buoyancy-driven forces that typically enhance fluid motion near the stretching sheet. The simulation results further indicate that as R increases, the thermal field declines, as shown in Figure 19. This suggests that higher radiation levels enhance thermal energy dissipation, leading to an overall reduction in fluid temperature. The thermal boundary layer becomes thinner with increasing R, likely due to enhanced radiative cooling effects dominating over internal heat generation or absorption. Interestingly, the simulation results show that increasing R results

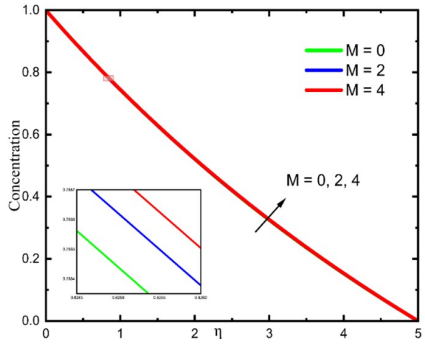

Figure 17: Variation of M on Concentration

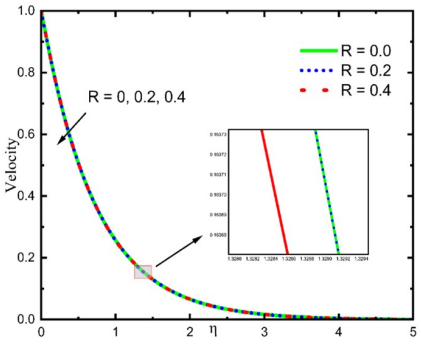

Figure 18: Variation of R on Velocity

in higher concentration levels, as depicted in Figure 20. The reduction in temperature appears to suppress thermal diffusion, allowing mass diffusion to dominate. This leads to a thicker solutal boundary layer and increased solute concentration near the sheet. The rise in concentration with higher R highlights the interplay between thermal and solutal transport processes in the fluid. The increase in Prandtl number (Pr) indirectly affects

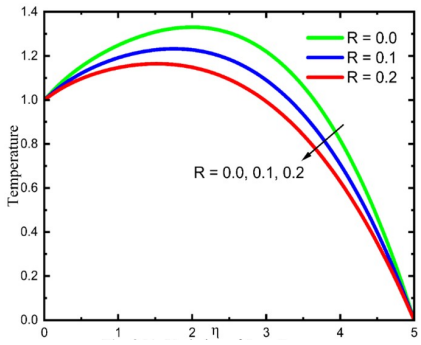

Figure 19: Variation of R on Temperature

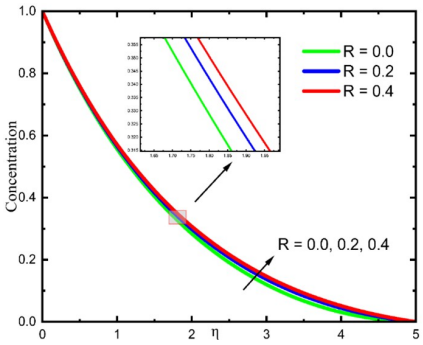

Figure 20: Variation of R on Concentration

the velocity profile. As the thermal boundary layer becomes thinner with higher Pr, the fluid experiences less thermal buoyancy, resulting in a slight decline in velocity near the sheet, as shown in Figure 21. This effect, though less pronounced than its impact on the temperature profile, illustrates the coupling between thermal and momentum transport processes. The results also indicate that as Pr increases, the temperature field rises, as shown in Figure 22. This unusual trend can be attributed to the fluid's specific heat and thermal properties. While higher Pr values typically reduce thermal diffusivity, in this case, the increase in Pr appears to enhance heat retention in the fluid, leading to a thicker thermal boundary layer and elevated temperature levels. This behavior is likely due to the dominant effect of viscous dissipation or other localized thermal sources within the system. The concentration profile decreases with increasing Prandtl number (Pr), as depicted in

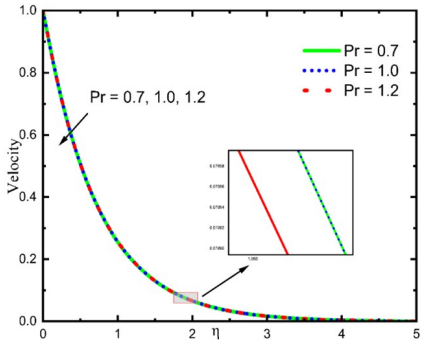

Figure 21: Variation of Pr on Velocity

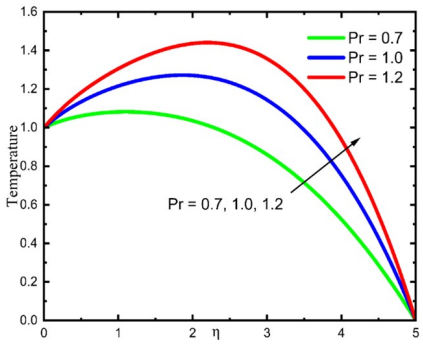

Figure 22: Variation of Pr on Temperature

Figure 23. Higher Pr values enhance thermal effects while reducing the dominance of mass diffusion (Dufour effect). This results in a thinner solutal boundary layer, as the solute disperses more effectively into the surrounding fluid, leading to lower concentration levels

near the sheet. The coupling between mass and heat transfer processes plays a critical role in this behavior. The heat source ($Q > 0$) or sink ($Q < 0$) parameter plays a crucial role

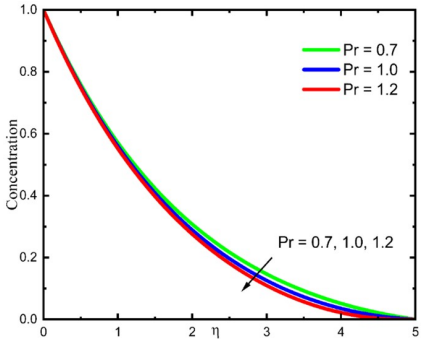

Figure 23: Variation of Pr on Concentration

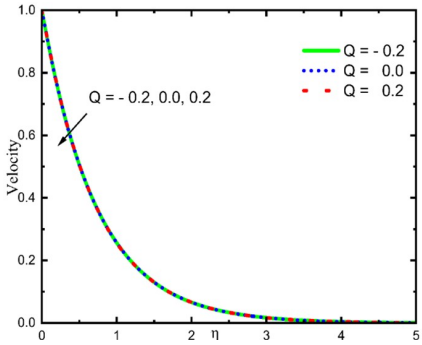

Figure 24: Variation of Q on Velocity

in regulating energy exchange within the hyperbolic tangent fluid. Since we are studying a hyperbolic tangent fluid (a non-Newtonian fluid), the viscosity may vary nonlinearly with the shear rate. Non-Newtonian fluids often exhibit complex responses to thermal and flow conditions, which may result in a damping effect that moderates the influence of heat emission or absorption on the velocity profile. The yield stress and viscoelastic properties of the fluid could lead to a more stable velocity profile that is less sensitive to thermal variations compared to Newtonian fluids, as explored in Figure 24. Its influence on the

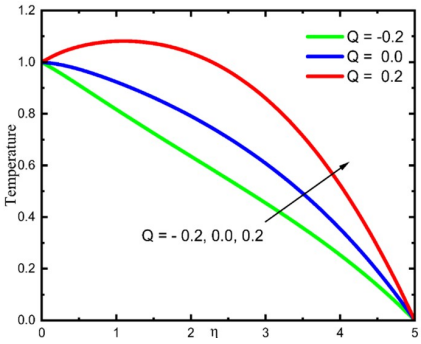

Figure 25: Variation of Q on Temperature

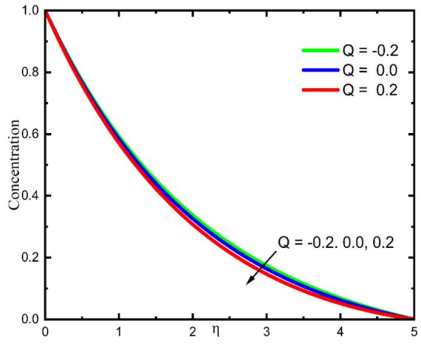

Figure 26: Variation of Q on Concentration

temperature profile is outlined in Figure 25, where a heat source ($Q > 0$) significantly increases the temperature due to enhanced thermal energy input, leading to a thicker thermal boundary layer. Conversely, a heat sink ($Q < 0$) reduces the temperature by dissipating thermal energy, resulting in a thinner thermal boundary layer. The sensitivity of the temperature field to Q highlights the critical role of energy supply or removal in controlling thermal dynamics. The concentration profile is also influenced by Q due to the coupling between mass and heat transfer. For a heat source ($Q > 0$), the enhanced thermal diffusion (Soret effect) tends to reduce concentration near the sheet, as shown in Figure 26. This leads to a thinner solutal boundary layer as solute particles disperse more effectively. On the other hand, a heat sink ($Q < 0$) lowers thermal energy, sup-

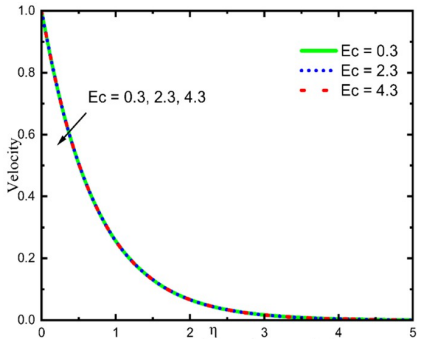

Figure 27: Variation of Ec on Velocity

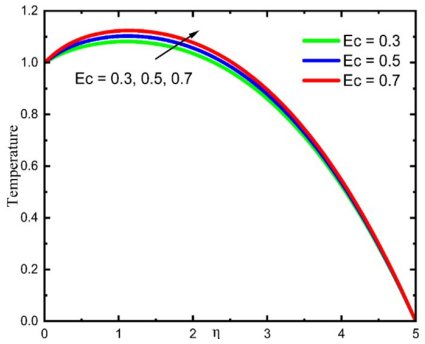

Figure 28: Variation of Ec on Temperature

pressing thermal diffusion and allowing mass diffusion to dominate, resulting in a higher concentration and a thicker solutal boundary layer. The Eckert number (Ec), which quan-

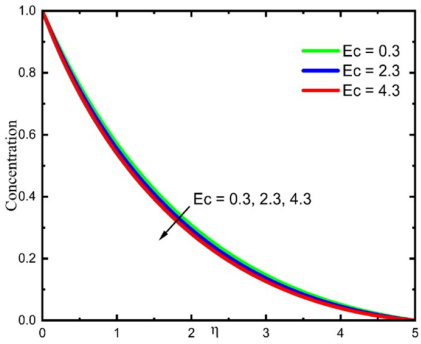

Figure 29: Variation of Ec on Concentration

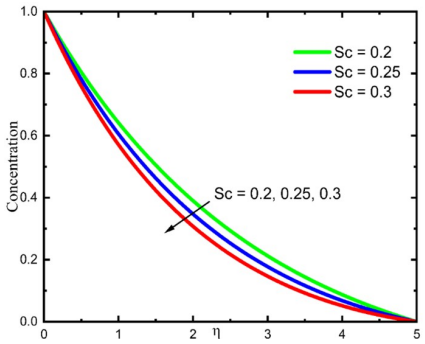

Figure 30: Variation of Sc on Concentration

tifies the conversion of kinetic energy into thermal energy, further decreases the velocity and amplifies the temperature profile, as observed in Figures 27 and 28. These findings are crucial for applications such as thermal management and energy systems. While the effect could be more complex depending on the Soret and Dufour effects and other transport phenomena, in general, as Ec increases, the concentration profile near the surface decreases due to increased thermal diffusion. This leads to a more uniform distribution of solute particles, as shown in Figure 29. The Schmidt number (Sc), representing the ratio of momentum diffusivity to mass diffusivity, significantly influences concentration distribution. Figure 30 shows that higher Sc values suppress mass diffusion, leading to a sharper concentration gradient and a thinner solutal boundary layer. This occurs because larger Sc values correspond to reduced mass diffusivity, limiting the spread of solute molecules. Such behavior is essential in applications requiring controlled mass transfer, such as in chemical reactors and separation processes. Figure 31 shows that increasing the Soret number (Sr) reduces the temperature and the thickness of the associated thermal boundary layer. This behavior is attributed to the fact that higher Sr inhibits thermal diffusion, thereby lowering the temperature profile. In contrast, the impact of the Soret number on the concentration field is opposite. As depicted in Figure 32, increasing Sr enhances the redistribution of species due to temperature gradients, resulting in increased

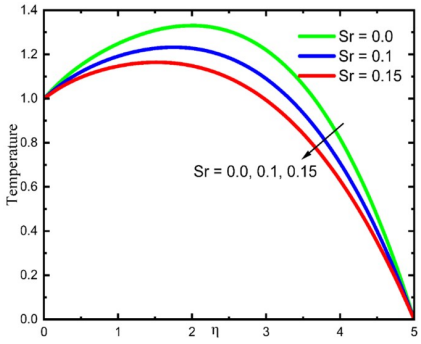

Figure 31: Variation of Sr on Temperature

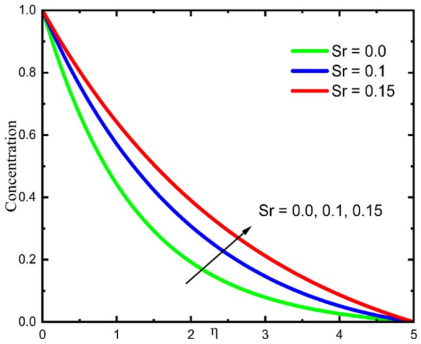

Figure 32: Variation of Sr on Concentration

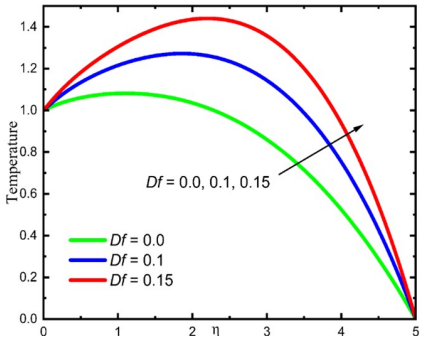

Figure 33: Variation of Df on Temperature

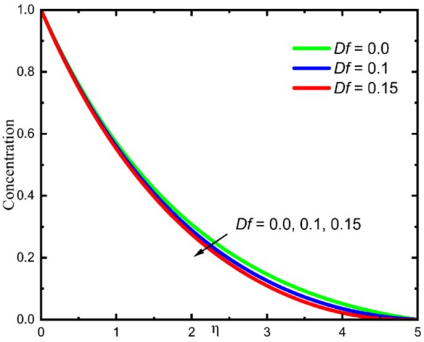

Figure 34: Variation of Df on Concentration

concentration and thickening of the solutal boundary layer. This contrasting behavior highlights the dual role of the Soret effect: simultaneously reducing temperature while increasing concentration due to thermal-concentration coupling. Figure 33 demonstrates

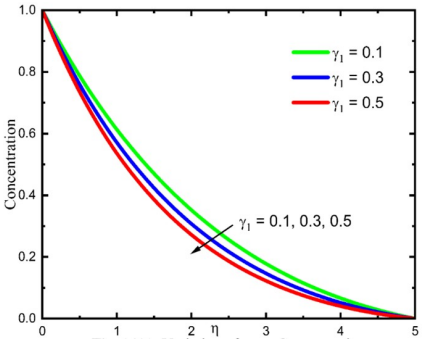

Figure 35: Variation of γ_1 on Concentration

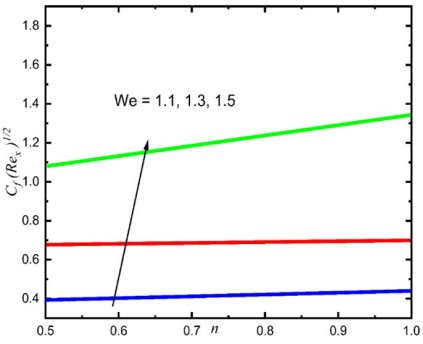

Figure 36: The effect of n and We on C_f

that increasing the Dufour number (Df) causes a rise in temperature. A greater Df strengthens the connection between momentum and heat transfer, substantially influencing the temperature distribution and possibly modifying heat transport patterns in the system. The effect of the Dufour number on the concentration profile reveals a complex relationship between heat and mass transport, as illustrated in Figure 34. An increase

in Df typically indicates stronger thermal diffusion, where heat energy influences mass transfer. This interaction decreases concentration at the surface, as enhanced thermal diffusion leads to more uniform solute distribution across the flow field. Consequently, a higher Dufour number results in a thinner concentration boundary layer. This behavior emphasizes the inverse relationship between the Dufour effect (heat affecting mass transport) and the Soret effect (mass influenced by thermal gradients), illustrating the intricate dynamics of transport mechanisms in non-Newtonian fluids.

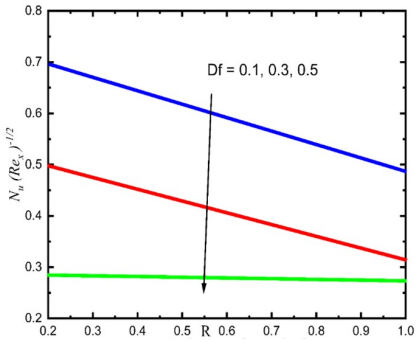

Figure 37: The impact of R and Df on Nu

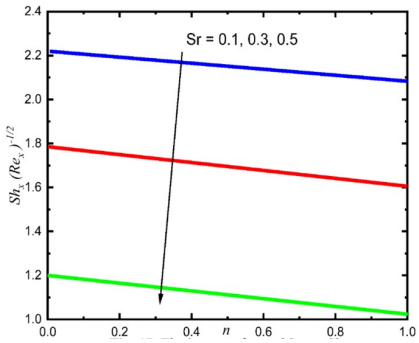

Figure 38: ThThe impact of n and Sr on Sh_x

The chemical reaction parameter (γ_1) has a significant impact on the concentration profile by introducing reactive mass transfer effects. As depicted in Figure 35, increasing γ_1 reduces concentration levels across the domain, with a noticeable thinning of the solutal boundary layer. This is due to enhanced chemical reactivity consuming solute species, thereby lowering overall concentration. These results are particularly relevant for chemically reactive systems, where control over the reaction rate is essential for optimizing mass transport.

Figure 36 illustrates the effect of the power-law index (n) and Weissenberg number (We) on the skin friction coefficient (C_f), demonstrating that C_f increases with rising values of both n and We. Figure 37 explores the effects of radiation (R) and Dufour number (Df) on the local Nusselt number (Nu_x), showing that Nu_x decreases as both R and Df increase. Lastly, Figure 38 exhibits that as n and Sr values increase, the local Sherwood number (Sh_x) decreases.

4. Conclusion

This work analyzes the two-dimensional effects of tangent hyperbolic fluid (THF) inclined magnetohydrodynamic (MHD) flow, viscous dissipation, power-law index, radiation, Soret and Dufour effects. The main conclusions of the analysis are summarized below.

Summary of Findings

- **Velocity:** Reduced by higher power-law index (n), magnetic field strength (M), inclination angle (γ), Eckert number (Ec), and Weissenberg number (We). The

combined effects of magnetic damping, gravitational resistance, elastic memory, and viscous dissipation contribute to the retardation of fluid motion. This understanding is crucial in designing systems where flow control, thermal regulation, or drag reduction is desired. These influences aid in optimizing industrial and biomedical applications involving non-Newtonian nanofluids.

- **Temperature:** Enhanced by Prandtl number (Pr), heat source ($Q > 0$), Dufour number (Df), and Eckert number (Ec), while reduced by higher radiation (R) and Soret number (Sr). The temperature distribution in a tangent hyperbolic nanofluid is governed by energy addition mechanisms (e.g., heat source, viscous dissipation, Dufour effect) and energy loss mechanisms (e.g., radiation, Soret-driven diffusion). Understanding these opposing effects is essential for thermal management in advanced systems such as nanofluid-based cooling devices, biomedical treatments, and porous media heat exchangers.
- **Concentration:** Increased by Soret number (Sr), but decreased by higher Schmidt number (Sc), Eckert number (Ec), and chemical reaction parameter (γ_1). The concentration of nanoparticles in a tangent hyperbolic nanofluid is shaped by a balance between thermal-driven diffusion (Soret effect) and restrictive or consumptive mechanisms such as viscous heating (Eckert number), limited diffusivity (Schmidt number), and chemical reactions. Understanding these factors is crucial for controlling nanoparticle distribution in bioengineering, chemical processing, and energy systems where precise mass transport is required.
- **Skin Friction:** Higher values of n and We lead to an increase in the skin friction coefficient (C_f).

These results provide critical insights into the interplay of physical parameters on the flow, heat, and mass transfer characteristics of hyperbolic tangent fluids. The findings have direct implications for industrial processes, energy systems, and environmental engineering involving non-Newtonian and nanofluid-based systems.

Author Contributions

All authors made substantial contributions to the manuscript.

Conflict of Loyalty Statement

The authors declare that no monetary investments or private connections exist or influenced the research presented in this paper, maintaining the highest standards of integrity and objectivity.

Data Availability

This article is a theoretical/conceptual piece and all the data is available in the article.

References

[1] A. K. Verma, A. K. Gautam, K. Bhattacharyya, A. Banerjee, and A. J. Chamkha. Boundary layer flow of non-newtonian eyring–powell nanofluid over a moving flat plate in darcy porous medium with a parallel free-stream: Multiple solutions and stability analysis. *Pramana*, 95(4):173, December 2021.

[2] M. M. Bhatti, M. A. Yousif, S. R. Mishra, and A. Shahid. Simultaneous influence of thermo-diffusion and diffusion-thermo on non-newtonian hyperbolic tangent magnetised nanofluid with hall current through a nonlinear stretching surface. *Pramana*, 93(6):88, December 2019.

[3] S. Saha and S. R. Kallem. Comment on: 'fluid flow and heat transfer characteristics of natural convection in square cavities due to discrete source-sink pairs'. *International Journal of Heat and Mass Transfer*, 235:126169, December 2024.

[4] C. G. Pavithra, B. J. Gireesha, S. Sushma, and K. J. Gowtham. Analysis of convective-radiative heat transfer in dovetail longitudinal fins with shape-dependent hybrid nanofluids: a study using the hermite wavelet method. *Applied Mathematics and Mechanics*, 46(2):357–372, February 2025.

[5] K. Karthik et al. Computational analysis of water-based silver, copper, and alumina hybrid nanoparticles over a stretchable sheet embedded in a porous medium with thermophoretic particle deposition effects. *Nanotechnology Reviews*, 13(1), August 2024.

[6] R. Lakshmi, B. J. Gireesha, P. Venkatesh, and K. J. Gowtham. Hermite wavelet approach to analyze the entropy generation of mhd williamson hybrid nanofluid flow through an inclined channel with particle shape effects. *International Journal of Applied and Computational Mathematics*, 11(2):40, April 2025.

[7] A. Mahdy and A. J. Chamkha. Unsteady mhd boundary layer flow of tangent hyperbolic two-phase nanofluid of moving stretched porous wedge. *International Journal of Numerical Methods for Heat & Fluid Flow*, 28(11):2567–2580, October 2018.

[8] S. M. Atif, S. Hussain, and M. Sagheer. Heat and mass transfer analysis of time-dependent tangent hyperbolic nanofluid flow past a wedge. *Physics Letters A*, 383(11):1187–1198, March 2019.

[9] S. Nadeem and N. S. Akbar. Series solutions for the peristaltic flow of a tangent hyperbolic fluid in a uniform inclined tube. *Zeitschrift für Naturforschung A*, 65(11):887–895, November 2010.

[10] S. Akram and S. Nadeem. Effects of partial slip on the peristaltic transport of a hyperbolic tangent fluid model in an asymmetric channel. *Computational Mathematics and Mathematical Physics*, 55(11):1899–1912, November 2015.

[11] B. J. Gireesha and K. J. Gowtham. Entropy generation analysis of hyperbolic tangent fluid in upright microchannel with hall effect by taylor wavelet collocation method. *International Journal of Ambient Energy*, 46(1):2495825, December 2025.

[12] N. S. Akbar, S. Nadeem, R. U. Haq, and Z. H. Khan. Numerical solutions of magnetohydrodynamic boundary layer flow of tangent hyperbolic fluid towards a stretching sheet. *Indian Journal of Physics*, 87(11):1121–1124, November 2013.

[13] M. Y. Malik, T. Salahuddin, A. Hussain, and S. Bilal. Mhd flow of tangent hyperbolic fluid over a stretching cylinder: Using keller box method. *Journal of Magnetism and Magnetic Materials*, 395:271–276, 2015.

[14] M. Waqas, G. Bashir, T. Hayat, and A. Alsaedi. On non-fourier flux in nonlinear stretching flow of hyperbolic tangent material. *Neural Computing and Applications*, 31(S1):597–605, 2019.

[15] K. U. Rehman, A. A. Malik, M. Y. Malik, and N. Ul Saba. Mutual effects of thermal radiations and thermal stratification on tangent hyperbolic fluid flow yields by both cylindrical and flat surfaces. *Case Studies in Thermal Engineering*, 10:244–254, 2017.

[16] K. Bashettahalli Ranganath et al. Investigation of squeeze film characteristics between a sphere and a flat plate in the presence of porous medium: Rabinowitsch fluid model. *ZAMM - Journal of Applied Mathematics and Mechanics / Zeitschrift für Angewandte Mathematik und Mechanik*, 105(5), 2025.

[17] K. T. Kumar et al. A numerical study on the radiative heat transfer aspects of hybrid nanofluid flow past a deformable rotating cone. *Multiscale and Multidisciplinary Modeling, Experiments and Design*, 7(6):5719–5729, 2024.

[18] T. Salahuddin, M. Y. Malik, A. Hussain, S. Bilal, and M. Awais. Effects of transverse magnetic field with variable thermal conductivity on tangent hyperbolic fluid with exponentially varying viscosity. *AIP Advances*, 5(12), 2015.

[19] M. V. Varsha et al. Electromagnetic mixed convective flow of dusty hyperbolic tangent hybrid nanofluid over a stretching surface: A quadratic regression analysis using rsm. *International Journal of Thermofluids*, 23:100803, 2024.

[20] M. Azam, T. Xu, and M. Khan. Numerical simulation for variable thermal properties and heat source/sink in flow of cross nanofluid over a moving cylinder. *International Communications in Heat and Mass Transfer*, 118:104832, 2020.

[21] M. Bibi, A. Hamid, and S. Tehseen. Automated skin lesion detection towards melanoma. *ICST Transactions on Scalable Information Systems*, page 159800, jul 2018.

[22] M. Shutaywi, M. Rooman, M. A. Jan, N. Vrinceanu, Z. Shah, and W. Deebani. Entropy generation and thermal analysis on mhd second-grade fluid with variable thermophysical properties over a stratified permeable surface of paraboloid revolution. *ACS Omega*, 7(31):27436–27449, 2022.

[23] A. Patra, M. K. Nayak, and A. Misra. Effects of non-uniform suction, heat generation/absorption and chemical reaction with activation energy on mhd falkner-skan flow of tangent hyperbolic nanofluid over a stretching/shrinking edge. *Journal of Applied and Computational Mechanics*, 6(3):640–652, 2020.

[24] Z. Ullah, G. Zaman, and A. Ishak. Magnetohydrodynamic tangent hyperbolic fluid flow past a stretching sheet. *Chinese Journal of Physics*, 66:258–268, 2020.

[25] I. S. Oyelakin and P. Sibanda. Analysis of exponentially varying viscosity and thermal conductivity on a tangent hyperbolic fluid. *SeMA Journal*, 77(3):257–273, 2020.

[26] K. Ganesh Kumar, A. Baslem, B. C. Prasannakumara, J. Majdoubi, M. Rahimi-Gorji, and S. Nadeem. Significance of arrhenius activation energy in flow and heat transfer of tangent hyperbolic fluid with zero mass flux condition. *Microsystem Technologies*,

26(8):2517–2526, 2020.

[27] N. F. M. Noor and I. Hashim. Mhd viscous flow over a linearly stretching sheet embedded in a non-darcian porous medium. *Journal of Porous Media*, 13(4):349–355, 2010.

[28] N. A. Ramly, S. Sivasankaran, and N. F. M. Noor. Zero and nonzero normal fluxes of thermal radiative boundary layer flow of nanofluid over a radially stretched surface. *Scientia Iranica*, pages 0–0, 2017.

[29] A. M. Amer, S. A. S. Al Rashdi, N. I. Ghoneim, and A. M. Megahed. Tangent hyperbolic nanofluid flowing over a stretching sheet through a porous medium with the inclusion of magnetohydrodynamic and slip impact. *Results in Engineering*, 19:101370, 2023.

[30] S. R. Kallem, S. R. Sheri, S. Gollapalli, and A. P. Perli. Numerical analysis on effect of soret number and inclined mhd of hyperbolic tangent fluid drift above an angled stretching panel in permeable material. *Multiscale and Multidisciplinary Modeling, Experiments and Design*, 8(5):227, 2025.

[31] A. A. Pasha, K. Irshad, S. Algarni, T. Alqahtani, and M. Waqas. Analysis of tangent-hyperbolic rheological model considering nonlinear mixed convection, joule heating and soret-dufour aspects from a stretchable convective stratified surface. *International Communications in Heat and Mass Transfer*, 140:106519, 2023.

[32] I. Ahmed, M. Alghamdi, M. Amjad, F. Aziz, T. Akbar, and T. Muhammad. Numerical investigation of mhd flow of hyperbolic tangent nanofluid over a non-linear stretching sheet. *Heliyon*, 9(7):e17658, 2023.

[33] S. R. Kallem, S. R. Sheri, G. Shankar, A. Prathiba, and M. Sunitha. Numerical investigation of the effects of radiation and heat source on the mhd flow of hyperbolic tangent fluid over a non-linear stretching sheet embedded in a porous. *CFD Letters*, 17(10):1–16, 2025.

[34] S. Sushma, C. G. Pavithra, K. J. Gowtham, and B. J. Gireesha. Impact of similarity transformations on hybrid nanofluid thermal behavior with thermal radiation on nonlinear stretching surface via hermite wavelet transformations. *Radiation Effects and Defects in Solids*, pages 1–25, 2024.

[35] S. R. Kallem, S. R. Sheri, A. Prathiba, and G. Shankar. Numerical analysis of the effect of chemical reaction and heat source on mhd hyperbolic tangent fluid flow across a non-linear stretching sheet in a porous medium. *Archives of Thermodynamics*, 46(2):57–67, 2025.

[36] S. R. Kallem, S. R. Sheri, A. P. Perli, M. M. Helal, and A. Ismail. Numerical investigation of tangent hyperbolic nanofluid with stagnation point flow of irregular heat and darcy-forchheimer effects on stretching sheet. *Results in Engineering*, 27:105821, 2025.

[37] M. Waqas, M. R. Almutiri, B. Yagoob, H. Ahmad, and M. Bilal. Numerical analysis of mhd tangent hyperbolic nanofluid flow over a stretching surface subject to heat source/sink. *Pramana*, 98(1):27, 2024.

[38] F. Khalid, S. Jahan, N. Sadiq, K. U. Tariq, and M. R. Ali. The enhanced heat transfer and flow dynamics of tangent hyperbolic and newtonian nanofluids under

inclined variable magnetic field. *Results in Physics*, page 108031, 2024.